JOURNAL OF GEOPHYSICAL RESEARCH, VOL. 112, F03S12, doi:10.1029/2006JF000517, 2007

Erosive dynamics of channels incised by subsurface water flow

Alexander E. Lobkovsky,[1] Braunen E. Smith,[2] Arshad Kudrolli,[2] David C. Mohrig,[1] and Daniel H. Rothman[1]

Received 4 April 2006; revised 23 August 2006; accepted 18 October 2006; published 3 March 2007.

[1] We propose a dynamical model for channels incised into an erodible bed by subsurface water flow. The model is validated by the time-resolved topographic measurements of channel growth in a laboratory-scale experiment. Surface heights in the experiment are measured via a novel laser-aided imaging technique. The erosion rate in the model is composed of diffusive and advective components as well as a simple driving term due to the seeping water. Steady driving conditions may exist whenever channels are incised into a flat and level erodible bed by a water table replenished via steady (on average) rainfall. Under such steady driving conditions, the model predicts an asymptotically self-similar growing shape for the channel transects. Conversely, given a transect shape that evolved under steady driving conditions and an estimate of the erosion rate at the bottom of the channel, granular transport coefficients can be inferred from the static channel shape. We report an estimate of these transport coefficients for a system of ravines incised into unconsolidated sand in the Apalachicola River basin, Florida.

Citation: Lobkovsky, A. E., B. E. Smith, A. Kudrolli, D. C. Mohrig, and D. H. Rothman (2007), Erosive dynamics of channels incised by subsurface water flow, *J. Geophys. Res.*, *112*, F03S12, doi:10.1029/2006JF000517.

1. Introduction

[2] Fluvial erosion commonly results in formation and growth of channels [*Schumm et al.*, 1984]. Several aspects of channelization are of interest, including the channelization instability [*Montgomery and Dietrich*, 1988, 1992; *Forterre and Pouliquen*, 2003], growth of the channel network [*Dunne*, 1980; *Willgoose et al.*, 1991; *Howard*, 1994] and the dynamics on an isolated channel [*Dietrich and Dunne*, 1993]. Understanding erosive channel dynamics requires both the knowledge of water fluxes as well as an adequate model of the sediment transport. Channels act to focus the flow of water, either overland [*Horton*, 1945], or, ubiquitously but less commonly appreciated, beneath the surface [*Dunne*, 1990; *Baker et al.*, 1990]. Here we focus on the latter.

[3] From a physical point of view, the chief advantage of studying channels driven by subsurface water flow or seepage is that the focusing of the water fluxes depends mostly on the shape of the channel if the local hydrology is uniform. On the other hand, the focusing of overland flows depends on the topography of the basin which drains into the channel. Therefore, when driven by subsurface flows, it is possible to study isolated channels only weakly coupled to the evolution of the entire basin.

[4] The subsurface water flows, which obey the well-established Darcy's law, can be readily computed. A predictive model of a single channel, therefore, depends on a precise description of the sediment transport in the channel. Such a model should predict the evolution of the channel's shape. It should also allow the fundamental sediment transport properties to be inferred from a measurement of a static channel. The channel shape therefore carries a signature of the underlying sediment dynamics.

[5] Following Jaggar's pioneering experiment [*Jaggar*, 1908] many other experimental studies of erosive dynamics driven by subsurface flows have been performed. The previous studies such as those of *Kochel et al.* [1985], *Kochel and Piper* [1986], *Howard* [1988] and *Kochel et al.* [1988] were chiefly concerned with analogy to Martian valleys. Previous experimental work suggests that groundwater piracy plays a dominant role in the development of channels. *Howard and McLane* [1988] studied the rate of seepage erosion in a narrow two-dimensional flow tank and formulated a hypothesis regarding the control of the water table geometry on the longitudinal channel profile. *Howard* [1994, 1995] has carried out computer simulations of valley development by groundwater sapping.

[6] Our approach is to conduct well-characterized laboratory experiments in which laser-aided imaging is used to obtain the full time-resolved channel shape [see also *Ni and Capart*, 2006]. We use these unique dynamical data to develop a quantitative description of the evolving channel transects. It is precisely our ability to collect time-resolved

[1]Department of Earth, Atmospheric and Planetary Sciences, Massachusetts Institute of Technology, Cambridge, Massachusetts, USA.
[2]Department of Physics, Clark University, Worcester, Massachusetts, USA.

0148-0227/07/2006JF000517$09.00

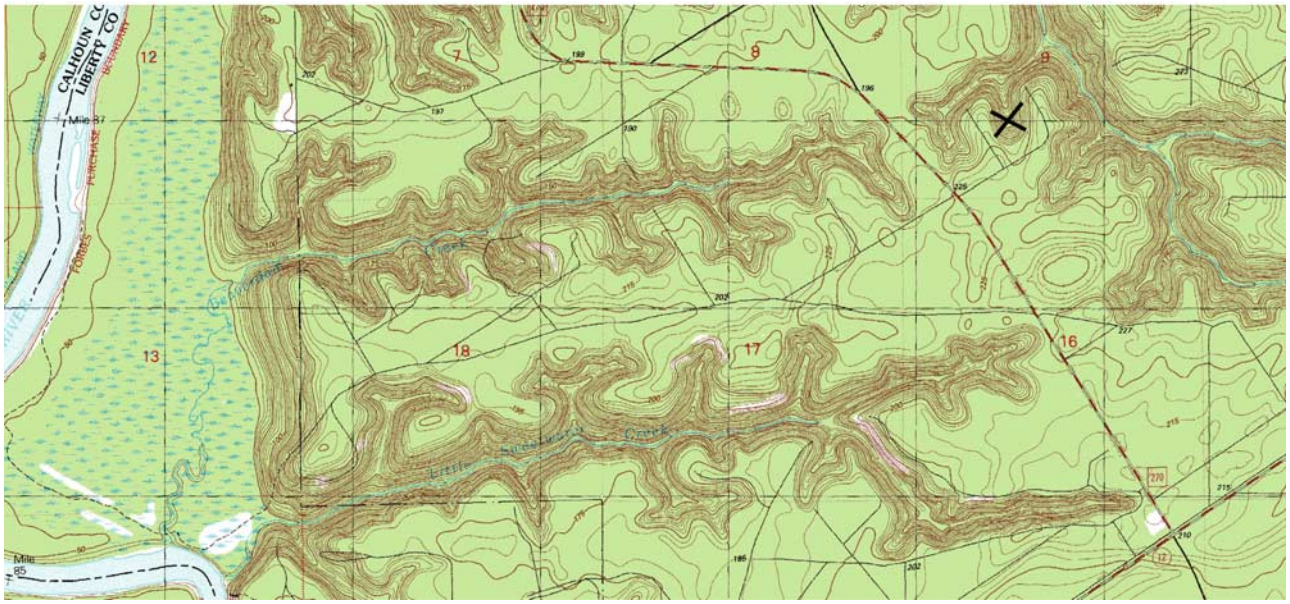

Figure 1. Contour map of approximately 20 km^2 area including branched sapping canyons in Liberty County, Florida. The channels are 20–50 m deep. As discussed in section 5, the marked channel was mapped with a laser range finder. (From the 1990 USGS map of the Bristol quadrangle, Florida. The 1000-m Universal Transverse Mercator grid provides the scale and the north (up) direction).

topographic information in the experiment that makes this kind of dynamic modeling possible. The main result of the modeling effort relates the erosion rate in the entire channel to (1) the erosion rate at the bottom, (2) a nonlinear relation between the uphill sediment advection rate and the slope, and (3) a diffusion constant. The resulting evolution equation, which is crafted for the specific case of subsurface driven erosion, predicts a characteristic growing channel shape. Although the qualitative mechanisms of seepage-driven channel dynamics have been understood for some time [*Dunne*, 1990], to our knowledge no previous study has yielded such quantitative predictions.

[7] The proposed evolution equation is coarse-grained because the time resolution of our height data is not sufficient to study the complicated grain-scale physics. The timescale relevant to our experiment is short compared with the time it takes to significantly alter the channel shape, but long compared to the time it takes for an avalanche front to propagate across the channel. A quantitative model based on the intermediate-scale measurements can be used to make important predictions for the evolving shape of the entire channel. Although it is obtained by averaging over many small-scale avalanches, our mesoscopic model still contains a signature of the microscopic granular dynamics [e.g., *Dietrich et al.*, 2003]. It can be used to constrain possible microscopic transport mechanisms and serve as a guide for selecting particular experimental regimes best suited for looking at the underlying microscopic granular dynamics.

[8] We test the predictions of our model in the remarkable network of channels located in the Apalachicola River basin near Bristol, in the western highlands of the Florida Panhandle. *Schumm et al.* [1995] suggest that these V-shaped valleys terminating in amphitheater heads are driven by groundwater sapping. Here we present a preliminary comparison with the model (a detailed description of the erosive processes at the field site is deferred to a future publication). The channels, examples of which are shown in Figure 1 are incised into the well-sorted unconsolidated sand of the Citronelle Formation. The infiltration capacity of this sand is high enough to preclude any overland water flow. We argue that the channels have been steadily driven by subsurface flows for a long enough time to reach an asymptotic state self-similar shape predicted by our model. We provide measurements to show that one of the channels is indeed well described by the asymptotic theory. From the fit and an estimate of the bottom erosion rate we are also able to extract all of the dynamical transport coefficients.

[9] In the next section we introduce our experimental apparatus and describe our method for acquiring the time-resolved topography. We detail our experimental procedure for growing a single channel and describe its morphology. We develop and test our model in section 3. The predictions of the model for the case of steady driving are explored in section 4. In section 5 we build the case for steady driving by discussing the network of sapping canyons in the Florida Panhandle. We also examine implications of the model's predictions for these canyons. Finally we summarize our results in section 6.

2. Experimental Method

[10] Figure 2 shows a schematic of our experimental apparatus, described in more detail elsewhere [*Schörghofer et al.*, 2004; *Lobkovsky et al.*, 2004]. Water enters beneath a pile of identical glass beads (mean diameter 0.5 mm, standard deviation 0.1 mm) through a square mesh of size 0.4 mm and exits at the foot of the pile through the same

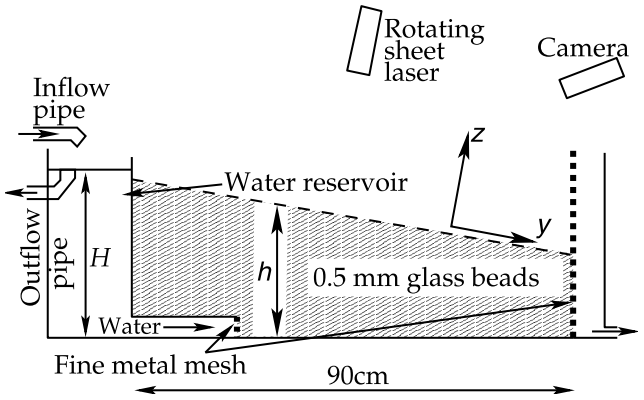

Figure 2. Schematic of our experimental setup. Constant head at the inlet mesh beneath the pile is maintained via an outflow pipe.

kind of mesh. The water flux is controlled by the height H of the water column in a reservoir behind the pile. The slope of the initial sandpile as well as the water column height are the control variables of the experiment. A scanning laser imaging technique allows us to measure the evolving height of the sandpile with grain-scale resolution in space and 1-min resolution in time. A laser sheet scans the surface once every minute while a digital camera acquires images from an oblique angle. The height of the surface is then extracted from an image of the intersection of the laser sheet with the granular surface. Resolution is limited by the laser light scattering off the rough surface of the pile. Specifically, the uncertainty in the measurement of the pile's height is 0.5 mm and the uncertainties in the x and y position measurements are 1 mm.

[11] *Schörghofer et al.* [2004] and *Lobkovsky et al.* [2004] describe the phenomenology of the pattern formation in this experiment and quantify the transitions between various modes of granular flow: surface flow (responsible for the formation of the channel network), slumping (bulk frictional instability) and fluidization. Here we focus on the evolution of an isolated channel grown from a small initial channel of triangular cross section. We are able to set the water level H in such a way that sediment is driven only in the channel. A contour map of a well-developed channel obtained with our laser imaging setup is shown in Figure 3. We find that the late stage morphology of the channel is insensitive to the exact initial condition as long as erosion occurs only within the incised channel. The initial incision must be sufficiently deep to guarantee that water level can be set at such a level that erosion only occurs within the incised channel and not on the surface of the pile.

[12] A well-developed channel evolves via small-scale avalanches in its head and bedload transport of the sediment through the valley. One-minute resolution in time is sufficient for a detailed study of the evolution of the channel's shape since a typical erosion rate is fractions of a grain diameter per minute. A typical avalanche front propagates across the head in a matter of seconds. Therefore our shape acquisition method yields the evolving topography averaged over many individual avalanches. The characterization of the channel shape on the timescale that is large compared to the avalanche timescale is useful for making predictions on the field scale, as exemplified by the Florida's sapping canyons discussed in section 5.

3. Experimental Results and Mesoscale Model

[13] The characteristic time τ_w for the relaxation of the water table toward its steady state position is of the order of the channel width $W \sim 10$ cm divided by the saturated hydraulic conductivity $K \approx 0.3$ cm/s (measured by *Schörghofer et al.* [2004]). Thus $\tau_w \sim 30$ s. On the other hand, the time τ_{ch} to significantly alter the shape of the channel is obtained by dividing the characteristic channel depth of 1 cm by the characteristic erosion rate of 0.02 cm/min yielding $\tau_{ch} \sim 3000$ s. Thus we can think of the water table adjusting instantaneously to changes in the channel shape.

[14] Our experimental study is directed at obtaining an expression for the erosion rate in the channel based on the analysis of the time-resolved topography measurements. We construct the expression for the erosion rate from considerations of symmetry and the assumption of self-similar channel growth delineated in the following three paragraphs and test it against the data. Such an approach is appealing since we do not need to consider the detailed grain-scale flow mechanisms and contend with a number of existing phenomenological approaches to modeling two-phase flow [e.g., *Yalin*, 1977]. Note also that the equation proposed below is specific to the case of erosion in a channel driven at the bottom.

[15] Let $h(x, y, t)$ denote the height of the pile measured relative to its surface before the channel forms. Thus h is identically zero before erosion sets in, negative in areas of net erosion, and positive in areas of net deposition. The height h is as a function of the cross-slope coordinate x, the downslope coordinate y, and time t. In general, the erosion rate $\partial h/\partial t$ depends on the local water and sediment fluxes, and features of the local topography, like the slope $|\nabla h|$, the curvature $\nabla^2 h$, etc. For an isolated channel, the shape of the water table and therefore the water fluxes are set by the shape $h(x, y, t)$ of the channel. The characteristic

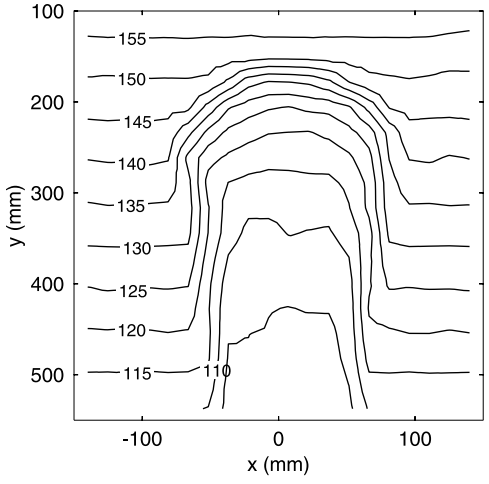

Figure 3. Contour map of a single channel after one hour of evolution for a pile of slope 7.8°. Contour labels are in millimeters.

timescale for the response of the sediment flux to the changes of the pile's shape is the time for a sediment particle to travel the length of the pile. The observed sediment velocities in our experiment are at least several millimeters per second. Thus the sediment flux adjusts quickly to the changes in the pile's shape.

[16] Since all of the factors which set the local erosion rate are determined by the shape $h(x, y, t)$ of the pile's surface, we seek an expression for the erosion rate $\partial h/\partial t$ in terms of h, its spatial derivatives and, possibly, integrals. In general, the local water and sediment fluxes depend on the shape of the entire pile. Thus, in general, there is a global dependence of the erosion rate on the surface shape. We argue that when the channel grows in a self-similar manner, the global dependence on the shape can be replaced by a single scale factor which characterizes the channel size. We therefore assume that channels grow in a self-similar manner and show below that this assumption is consistent with the experiment.

[17] So far we have argued that, when channels grow slowly and in a self-similar manner, the erosion rate is a function of the local topography h, its spatial derivatives, and an overall scale factor which we choose to be the depth $|h_0|$ of the channel. We simplify the problem further by focusing on the evolution of transverse channel sections. We therefore focus on the dependence of the erosion rate on derivatives of h with respect to the transverse coordinate x only. Variation of the water flow in the downslope y direction is accounted for via y-dependent coefficients. This approximation is reasonable everywhere except the leading portion of the channel's head where the direction of the downslope gradient varies rapidly. Grains and microscopic avalanches enter and leave any given channel transect. Projected onto this transect, the transport of height h is no longer volume conserving.

[18] The expression for the erosion rate should contain terms which represent driving as well as transport. Transport terms can in general be diffusive or advective. Diffusive granular transport has been observed in the field [*McKean et al.*, 1993] and has long been considered a major process [*Culling*, 1960]. We therefore include h_{xx} in our equation (subscripts denote differentiation). Advective transport, which is nonlinear in general, is represented by some function of h_x. Erosive driving due to seeping water should depend on the overall scale factor h_0. Since we assume that the channel and therefore the shape of the water table evolves in a roughly self-similar manner, the driving term can only depend on h/h_0. We therefore propose that

$$h_t = \nu h_{xx} - \delta|h_x| - \lambda h_x^2 - \mu\Theta(h/h_0 - f), \qquad (1)$$

where the Heaviside theta function is defined by $\Theta(z) = 1$ if $z > 0$ and $\Theta(z) = 0$ otherwise. The empirical constants μ, ν, λ, δ, and f are functions of time t and downslope coordinate y. They encode the microscopic properties of the grain dynamics as well as the strength of the driving water flow. The diffusion constant ν reflects the rate of smoothing of local perturbations. The last term on the right hand side represents driving due to the seeping water. We assume that the effect of the seeping water is to add a constant μ to the erosion rate when the local depth h is greater than a fraction f of the channel depth h_0. Whereas other choices for the driving term are possible, an additive constant erosion rate below the intersection of the water table with the channel is perhaps the simplest. Our data are sufficiently noisy to preclude a possibility of a quantitative comparison between different choices for the driving term. As we will see below, as long as the driving term is a function of h/h_0 only, the channel shape tends toward a self-similar solution.

[19] The second and third terms on the right hand side of (1) are advective. We hypothesize, in accord with *Boutreux et al.* [1998], that perturbations are advected only up the slope. $\delta|h_x|$ corresponds to advection of perturbations with velocity δ independent of slope, whereas λh_x^2 corresponds to advection with velocity $\lambda|h_x|$, which grows linearly with slope.

[20] As mentioned in the introduction, the time resolution of our experimental data are insufficient to make contact with the underlying microscopic dynamics (e.g., avalanches). Although this precludes development of a microscopically based transport theory, we show below that our macroscopic phenomenological description nevertheless allows us to connect channel geometry to the transport coefficients.

[21] To establish that equation (1) is a good representation of the erosion rate in our experiment, we measure a number of points h^i in a narrow window in time and a window in the downslope coordinate y shown in Figure 5. For each location i in this space-time window we compute the space derivatives h_x^i and h_{xx}^i and the time derivatives h_t^i of the height and fit the resulting data cloud via least squares to equation (1). More specifically, we minimize the sum $F = \sum_i (h_t^i - \nu h_{xx}^i + \delta|h_x^i| + \lambda(h_x^i)^2 + \mu\Theta(h^i/h_0 - f))^2$ over the space-time window with respect to the variation of the five parameters ν, δ, λ, μ, and f. Because F has many local minima, we use the method of simulated annealing [*Press et al.*, 1986, and references therein] to find the global minimum of F in the five-parameter space. Although the errors and the correlations between the values of the parameters which globally minimize F, can be obtained by computing the joint distribution of the parameters in equilibrium at some temperature, we did not compute them.

[22] In Figure 4 we illustrate the relative importance of the advective, diffusive and driving terms by plotting their respective contributions to the erosion rate. As shown in Figure 4a, the advective terms make the largest contribution to the erosion rate with the nonlinear term (λ) comparable to the linear term (δ). Data points with slopes smaller than 0.7, comprising over 95% of all data, have been used in the fit. A discrepancy between the model and the data occurs for larger slopes where the erosion rate saturates. A measurable contribution to the erosion rate due to diffusion is shown in Figure 4b. While the extracted positive granular diffusivity ν is statistically significant, diffusion is a negligible source of the erosion rate. The driving, depth-dependent term, shown in Figure 4c, is approximated by a step function although the data show perhaps a more gradual transition. For steady driving, discussed further below, we expect the width of the transition region to remain constant.

[23] The picture that emerges is of a channel driven below a certain fraction of its depth resulting in nonlinear uphill advection of heights. As the channel grows, the step-function approximation to the driving term should improve

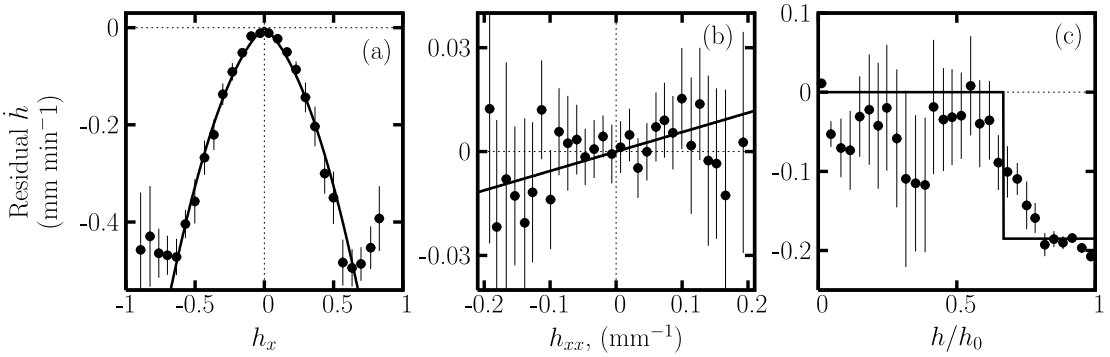

Figure 4. Partial erosion rate at $t = 39$ min plotted against (a) the slope, (b) the curvature, and (c) the fractional channel depth. Each symbol represents an average over several hundred data points. Partial erosion rate is obtained by subtracting from the measured $\dot{h}$ terms on the right hand side of equation (1) which depend on the variables other than the one against which the partial erosion rate is being plotted. For example, in Figure 4a we plot the measured $\dot{h}$ minus the diffusive and the driving terms calculated from the measured topography. Spatial derivatives of h were calculated using a smoothing scale ξ. We found that there exists a ξ intermediate between the grain size and the channel size, for which the fits do not depend on ξ. Lines are drawn using the parameters $\mu = 0.185$ mm^2/min, $\nu = 0.056$ mm/min, $\lambda = 0.818$ mm/min, $\delta = 0.244$ mm/min, $f = 0.67$ extracted by a least squares fit of the unbinned data to equation (1). Error bars represent two standard deviations of the mean.

with time. A different driving term, as long as it is a function of h/h_0 and is nonzero only below a fraction of the channel depth, changes the picture quantitatively but not qualitatively.

[24] We extracted model parameters near a transect, shown in Figures 5a and 5b, that is fixed with respect to the location of the water inlet. As the channel migrates up the slope, the geometry of the water flow changes. As a result, the model parameters, presented in Figure 6, evolve. The chosen transect is located initially ahead of the predug channel. As the channel head passes this transect, the driving rate μ peaks and then declines. The values of the effective advection speeds δ and λ also decrease since they are related to the driving. A possible explanation for the change in the effective advection speeds is that we are measuring advection averaged over many avalanches. As the driving, (i.e., the erosion rate at the channel's bottom) decreases, the avalanche frequency, and therefore the effective advection speed, decreases as well. The diffusion coefficient $\nu = 0.039 \pm 0.033$ mm^2/min (or 7×10^{-10} m^2/s) and the fractional driving $f = 0.52 \pm 0.14$ fluctuate around their respective means which are roughly time-independent. Large fluctuations in the extracted parameters reflect the underlying uncertainties in the measurement of the heights $h(x, y, t)$.

[25] As a consistency check of the model's validity, we should be able to use the extracted time-dependent model parameters to reproduce the evolution of the transect shape. Figure 7 compares the measured shapes of this transect with the shapes evolved via equation (1) with the time-dependent coefficients extracted by the least-squares fit. Agreement indicates that the right-hand side of equation (1) captures the essential features of the erosion rate in the channel geometry. In other words, the difference between the measured erosion rate and the inferred right-hand side of equation (1) is small and uncorrelated with any feature of the topography. The rate of advance of the channel sidewalls and the receding rate of the channel bottom are determined by different combinations of the parameters. The agreement of the shapes evolved via equation (1) with the experimental data shows that both rates are in accord with the experiment.

4. Steady Driving

[26] The model coefficients in our experiment, intimately related to the geometry of the water flow, change markedly during the evolution of the channel as illustrated in Figure 6. In other geometries these coefficients can remain approximately constant over a long time. As we argue in more detail in the following section, steady driving conditions exist in the array of seepage driven channels in the Florida Panhandle [*Schumm et al.*, 1995] that receive water from a water table curved by their presence. In this geometry, the water flux to the channel's head is determined only by the curvature of the

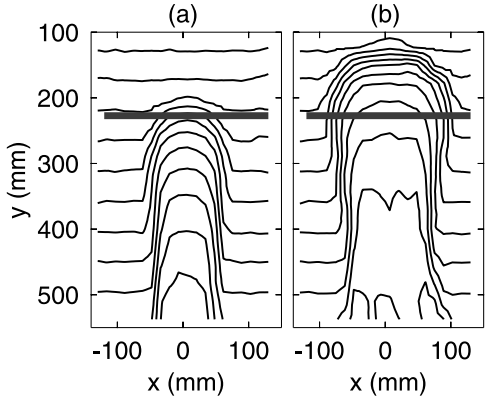

Figure 5. Contour plots of the laser height data at (a) 15 min and (b) 115 min after the start of the water flow. The thick line shows the transect from which the data are collected and used to extract the model parameters shown in Figure 6. Contour interval is 5 mm.

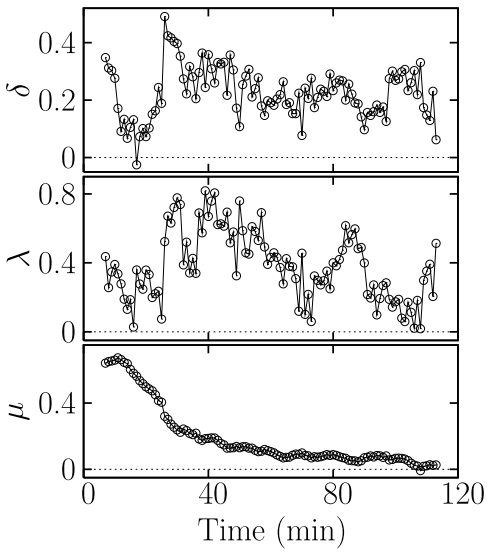

Figure 6. Example of the evolution of the coefficients μ, λ and δ (measured in mm/min) extracted using equation (1) from the data using taken near a fixed transect illustrated in Figure 5. The head of the channel arrives to this transect approximately 1 min after the start of the experimental run.

water table near the head and is thus independent of the channel head location. Consequently, the driving term in equation (1) is independent of the head location and hence time (on a timescale long enough to average over the variability of precipitation). It is therefore appropriate to examine the long-time behavior of equation (1) with constant coefficients. We show in Appendix A that an asymptotically self-similar solution exists when driving is steady. The resulting predictions for channel geometry are likely to be relevant to field-scale geologic problems.

[27] While relegating the details of the calculation to the appendix, we describe the main features of the asymptotic solution here. It turns out that after a time long compared to

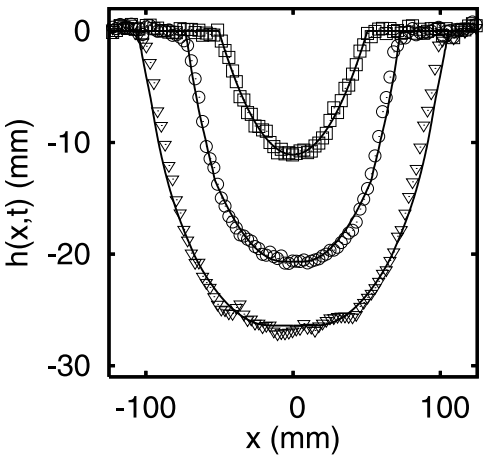

Figure 7. Measured height across the chosen transect at t = 15, 45, and 115 min compared to the prediction of equation (1). The smoothed shape of the transect at t = 15 min was used as the initial condition. Actual time-dependent parameters presented in Figure 6 were used.

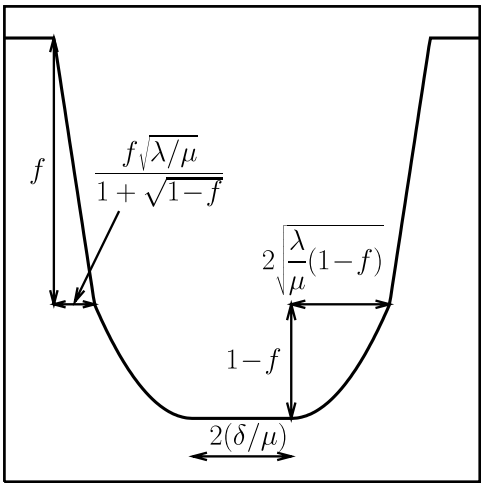

Figure 8. Vertically exaggerated illustration of the asymptotic channel shape. Flat bottom is joined onto parabolic flanks followed by straight flanks.

$\tau = \nu/\mu^2$, the channel shape "forgets" its initial condition and approaches a state in which its transects only increase in scale while retaining their overall shape. This self-similar solution implies that the channel depth d grows linearly with time at a rate μ, while the transect shape scaled by the depth h/d approaches a function $\eta_0(x/d)$ of the transverse coordinate x scaled by the depth d. As we show in the appendix, the shape function η_0 (see Figure 8) consists of a flat bottom, parabolic flanks in the driven region (below the point where the water table emerges into the channel) joined onto straight flanks of slope

$$s_0 = \sqrt{\mu/\lambda}\left(1+\sqrt{1-f}\right). \tag{2}$$

Since the channel is driven from below, this angle should correspond to the angle of repose of dry sand. The half-width W of the channel grows linearly at a rate

$$v = \frac{a\xi_e}{\tau} = \delta + \lambda s_0. \tag{3}$$

The asymptotic shape can be used successfully to fit channel cross sections in our experiment which evolve in nonsteady conditions. However, the ratios of parameters extracted by such an asymptotic fit deviate greatly from the parameters extracted by the fit of the equation (1) to the data cloud, because the shape of the channel at the time of the fit retains a memory of its prior dynamical state. The diffusive term acts to smooth the slope discontinuities at the edges of the channel. We are able to find an exact solution to equation (1) near these corners, thereby obtaining the characteristic radius of the smooth channel edges,

$$R = \frac{2\nu}{\sqrt{\lambda\mu}(1+\sqrt{1-f})}. \tag{4}$$

The self-similar solution connects the static profile of the channel, including the angle of repose, with the dynamic granular transport coefficients. Given a transect shape that

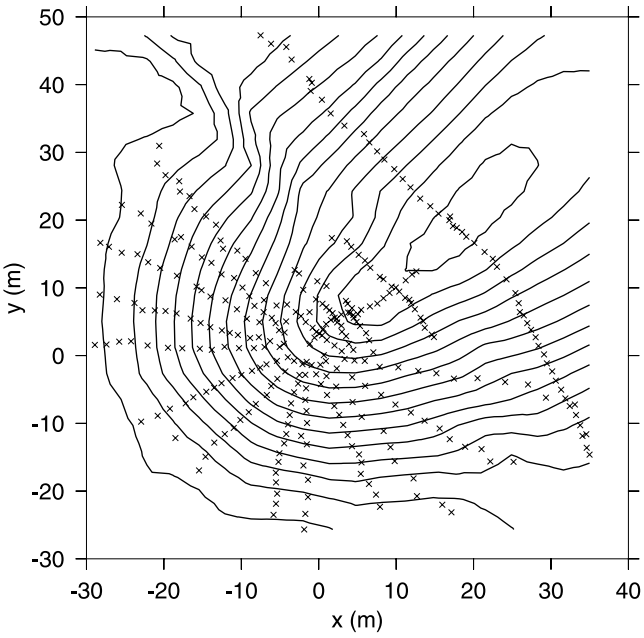

Figure 9. Contour map of the chosen channel's head. Contour interval is 1.5 m. We mark points at which the height measurements are taken.

has evolved under steady driving conditions, a fit to the asymptotic shape as well as the smooth edges yields f, λ/μ, δ/μ, and ν/μ. Thus an independent estimate of the bottom erosion rate μ is all that is required to recover all of the dynamic transport coefficients in the model.

5. Comparison With Field-Scale Seepage Channels

[28] Working in the Florida Panhandle, *Sellards and Gunter* [1918] (as cited by *Schumm et al.* [1995]) recognized that certain linear valleys were formed by spring sapping. A spring emerged at the base of amphitheater heads which terminated each valley. Recently, *Schumm et al.* [1995] have described in detail the characteristic features of the topography of these so called "steepheads." According to *Schumm et al.* [1995], these valleys are cut into the Plio-Pleistocene Citronelle Formation which consists of highly permeable well-sorted unconsolidated sand. Owing to the high infiltration capacities of Citronelle sands ranging from 8 to 12 inches per hour [*Overing and Watts*, 1989] (cited by *Schumm et al.* [1995]), virtually no overland water flow is observed. Rainwater therefore recharges the water table which emerges as spring heads at the bottom of the valleys. Drilling did not reveal inhomogeneities in the hydrology down to depths of several meters below the valley bottoms [*Schumm et al.*, 1995]. It is therefore likely that the dynamics and the morphology of the network of the "steepheads" is controlled purely by the dynamics of sand in the channels driven by the ground water seepage.

[29] We performed our own preliminary survey of the sapping canyons which drain into Apalachicola River. A USGS contour map of the canyons located on the Nature Conservancy's Apalachicola Bluffs and Ravines Preserve is shown in Figure 1. We verified the homogeneity of the sand layer (which extends down to approximately 100 feet below flat ground level) by granulometric measurements of samples taken from different parts of the slope. We mapped out the topography of the head of one of the channels (marked on Figure 1) using a laser range finder. The contour map together with the locations of the measurement points is presented in Figure 9. Lack of data in the left upper corner of the graph results in the distortion of the computed contours.

[30] We assume that shape of the channel has reached the asymptotic self-similar shape. For this to happen driving must be steady for at least time $\tau = \nu/\mu^2$. We estimate these parameters and then a posteriori justify the assumption of asymptotic shape. In Figure 10 we show the measured heights of the longest transect normal to the axis of the channel together with a fit to the asymptotic self-similar shape with smooth edges. The agreement is good except near the bottom, where presumably sediment is piled up following a sidewall slump. As a result the error in the estimate of δ/μ is rather large (30%). From the fit we obtain the dimensionless ratios $f \approx 1$, $\lambda/\mu \approx 2.8 \pm 0.2$, $\delta/\mu \approx 0.3 \pm 0.1$ and the smoothing scale $R \approx 10 \pm 1$ m of the channel's edges. Using expression (2) for the asymptotic flank, we obtain the slope of 31°, in good agreement with the angle of repose of dry sand.

[31] These results may be understood as follows. First, $f = 1$ because the average rainfall rate $r \sim 1.5$ m/year is such that even a small area of contact of the water table with the channel is sufficient to drain the rainfall into the channel. We estimate the extent ℓ of the sapping face by assuming that the slope of the water table near the channel is roughly equal to the slope s_0 of the channel wall. The resulting subsurface flow velocity Ks_0 is responsible for draining the rainfall flux rD, where $D \sim 100$ m is the half-distance between the channels. Thus $\ell Ks_0 \sim rD$ and therefore $\ell \sim rD/Ks_0 \approx 2$ cm. Since the channels are roughly 20 meters in depth, the fractional driving depth $f = (20.0 - 0.02)/20.0 \approx 1$ as expected.

[32] We also seek an independent estimate of the bottom erosion rate μ to obtain the advection speeds λ and δ. We

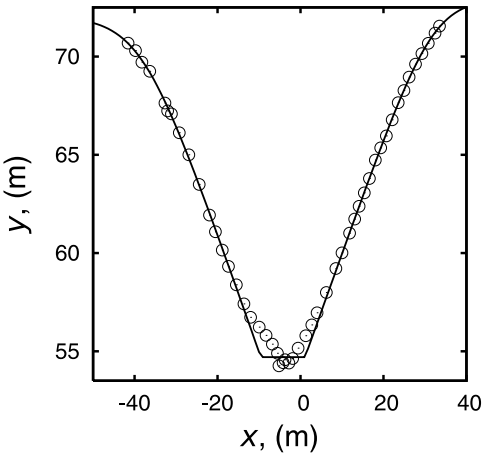

Figure 10. Measured height of the transect (symbols) fitted to the asymptotic transect shape with the smooth channel edges according to equations (A8) and (A11).

assume that the canyons came into existence around the same time as the Citronelle formation itself, i.e., around the Last Glacial Maximum in the sea level, or approximately 100,000 years ago [*Fleming et al.*, 1998]. In this time the channels reached a depth of roughly 50 meters where they join the Apalachicola River. Assuming that the channels grew at a roughly constant rate we estimate $\mu \approx 5 \times 10^{-11}$ m/s or about 0.5 mm/year. On the other hand the head advance rate can be estimated by assuming that it was constant throughout its history and resulted in 5 -km-long channels. It is thus about 100 times larger than the bottom erosion rate or about 5 cm/year. The weakest point of this argument is that it assumes that the Apalachicola River itself has not moved.

[33] The estimate of the bottom erosion rate is perhaps most useful for obtaining the value of the diffusion constant ν since other estimates of ν exist in the literature. By fitting the data to equation (A11) we find the radius of curvature of the channel's edge to be $R \approx 10$ m. This implies that the diffusion constant is $\nu \approx 7 \times 10^{-10}$ m^2/s, which is in agreement with the value of the diffusion constant we measure in our experiment. This value for ν is bracketed by estimates of 10^{-9} m^2/s for clay soils [*McKean et al.*, 1993] and of 2×10^{-10} m^2/s for granular soils [*Reneau et al.*, 1989]. Both works assumed purely diffusive transport. There is likely a strong dependence of the effective diffusion constant on the particle size as well as the precise nature of the dominant disturbance mechanism. Whereas in the tabletop experiment the flow of water and grains is the only such mechanism, other processes can dominate in the field. Examples of disturbance mechanisms which do not originate from subsurface water flow are rain or bioturbators (e.g., vegetation, burrowing animals [*Yoo et al.*, 2005]). It is unclear at this point whether the fact that we obtain the same value of the diffusivity in the field and in the experiment signals the dominance of the hydraulic processes originating in the subsurface water flow.

[34] Given an estimate of the granular diffusivity we can compute the characteristic time τ for reaching the asymptotic shape: $\tau = \nu/\mu^2 \approx 9000$ years. This time is an order of magnitude shorter than the apparent age of the channels. Therefore it is likely that the asymptotic self-similar state has been achieved.

[35] The estimate of the bottom erosion rate as well as the fit of the transect shape to the asymptotic shape also yields the values of the effective advection speeds $\delta \approx 1.5 \times 10^{-11}$ m/s and $\lambda \approx 1.4 \times 10^{-10}$ m/s. These values can be used to check the predicted channel half-width W using the channel edge velocity from equation (3). We find that $W \approx 100$ m which compares well with the observed half-width of the channels.

6. Discussion and Conclusions

[36] We conducted a laboratory experiment in which channels are incised into a granular bed by subsurface water flow. Using high-resolution topographic data obtained with a laser imaging system we constructed and tested an effective model for the evolution of channel transects. In this model, the erosion rate is composed of the local diffusive and nonlinear advective terms as well as a nonlocal driving term which depends on the overall depth of the channel. With constant coefficients, the evolution equation admits a unique asymptotic similarity solution. Thus, under steady driving conditions, the shape of the channel's transects approaches the characteristic form while growing with a constant rate. Thus the similarity solution affords a way of extracting dynamic information such as granular transport coefficients from a static shape of the channel that is known to have evolved under steady driving conditions. Conversely, the transport coefficients determine the asymptotic channel shape. In particular, the ratio of the nonlinear advection speed λ to the bottom erosion rate μ is directly related to the angle of repose of dry sand.

[37] When, as in our experiment, dynamic topographic information is available, the fit of the model to the data yields the values of the effective diffusivity ν, advection speeds δ and λ, and the bottom erosion rate μ. Since our description averages over individual avalanches, the transport coefficients reflect the average rate of transport on a long timescale. Thus they have more to do with the frequency and size distribution of the avalanches than the granular dynamics within an avalanche. In other words, our advection term $\delta|h_x|$ does not imply that a perturbation travels uphill at rate δ, but rather that over a time long compared to the characteristic interavalanche time, a perturbation migrates uphill with this rate as a result of many fast avalanches.

[38] We hypothesize that the sapping canyons incised into the Citronelle formation in the Florida Panhandle evolve under steady driving conditions, and show that the asymptotic self-similar state has likely been reached. Under these assumptions we are able to fit the channel shape to the asymptotic solution of our model. Together with an independent estimate of the bottom erosion rate μ we recover all transport coefficients in our model. The ability to extract dynamic information from a static shape with a minimal set of assumptions is the key strength of our model.

[39] The most natural next step is to extend the model to three dimensions. Owing to sediment conservation, the expression for the erosion rate in this case will have to be the divergence of the sediment flux. Armed with a plausible three-dimensional model, we expect to study the full channel shape including the geometry of the channel head, the channel's longitudinal profile, and the mechanism for the side-branching instability. An important component of any three-dimensional modeling will be understanding the geometry of the water table in the presence of the complicated network of channels. We expect several important conclusions to emerge from the computation of the seepage water fluxes. For example, a widely mentioned feature of networks driven by seepage is the large angle of tributary junctions [*Schumm et al.*, 1995]. We anticipate that a simple assumption that a tributary's head grows in the direction of maximum seepage flux coupled with a calculation of the water table curvature will yield a justification for this observation.

Appendix A: Calculation of the Asymptotic Channel Shape

[40] We first nondimensionalize equation (1) by scaling all lengths by $a = \nu/\mu$ and time by $\tau = \nu/\mu^2$ and defining $\beta = \delta/\mu$ and $\alpha = \lambda/\mu$. We use the same symbols for the

scaled variables h and t. The resulting nondimensionalized evolution equation reads

$$h_t = h_{xx} - \beta|h_x| - \alpha h_x^2 - \Theta(h/h_0 - f). \tag{A1}$$

We seek an asymptotically self-similar solution to equation (A1) by introducing a time-dependent scale factor $d(t)$ and the scaled shape $\eta(\xi, t) = h(x, t)/d(t)$, where $\xi = x/d(t)$. We can choose $d(t)$ in such a way that $\eta(0, t)_{t\to\infty} \longrightarrow 1$, so that $d(t)$ can be interpreted as the channel depth at long times. In anticipation of the asymptotic self-similar solution, we expand $\eta(\xi, t)$ and $d(t)$ in a power series in $1/t$. We obtain

$$\eta(\xi, t) = \eta_0(\xi) + \frac{1}{t}\,\eta_1(\xi) + \ldots \tag{A2}$$

$$d(t) = t + o(t), \tag{A3}$$

where $o(t)$ refers to a term which grows slower than t as $t \to \infty$. The zeroth order shape $\eta_0(\xi)$ is independent of time. Thus, if the expansion (A2) converges, the shape converges to the similarity solution $\eta_0(\xi)$. Substituting the expansion (A2) into equation (1) and collecting orders of $1/t$ we obtain at the lowest, time-independent, order,

$$\eta_0 - \xi\eta_0' = -\beta|\eta_0'| - \alpha(\eta_0')^2 - \Theta\left(\frac{\eta_0}{\eta_0(0)} - f\right), \tag{A4}$$

where primes denote differentiation with respect to ξ. Note that the diffusive term does not enter at the lowest order. The physical reason for this is that, as we show below, diffusion is important on a fixed length scale. As the channel grows larger than this diffusive length, the h_{xx} term in equation (A1) becomes negligible compared to the advection and the driving terms.

[41] The solution to equation (A4) must be symmetric with respect to $\xi \to -\xi$ and smooth everywhere except at the point ξ_0 of emergence of the water table where $\eta_0(\xi_0) = f\eta_0(0)$. It turns out that there exists a one-parameter family of similarity solutions which satisfy these criteria. These solutions are constructed as follows. In the driven region $|\xi| < |\xi_0|$, any piece of the parabola

$$\eta_0(\xi) = \frac{1}{4\alpha}\left(\xi^2 - 2\beta\xi + \beta^2 - 4\alpha\right), \tag{A5}$$

and a tangent line to this parabola at some arbitrary point ξ_1,

$$\eta_0(\xi) = \frac{1}{4\alpha}\left(2\xi(\xi_1 - \beta) + \beta^2 - \xi_1^2 - 4\alpha\right), \tag{A6}$$

are solutions to equation (A4) as can be verified by substitution. In the undriven region $|\xi| > |\xi_0|$, the trivial solution $h = 0$ as well as tangents to the parabola

$$\eta_0(\xi) = \frac{1}{4\alpha}\left(\xi^2 - 2\beta\xi\right) \tag{A7}$$

are solutions as verified by substitution. A smooth solution symmetric around $\xi = 0$ is therefore constructed from five pieces,

$$\eta_0 = \begin{cases} -1, & 0 < \xi < \xi_b, \\ -1 + \dfrac{(\xi - \xi_b)^2}{4\alpha}, & \xi_b < \xi < \xi_1, \\ -1 + \dfrac{(\xi_1 - \xi_b)^2}{4\alpha} + \dfrac{(\xi_1 - \xi_b)(\xi - \xi_1)}{2\alpha}, & \xi_1 < \xi < \xi_0, \\ -f + s_0(\xi - \xi_0), & \xi_0 < \xi < \xi_e, \\ 0, & \xi > \xi_e. \end{cases} \tag{A8}$$

The first piece is the flat bottom of the channel $\eta_0 = -1$ tangent to the parabola (A5) at its apex $\xi_b = \beta$. The second piece is part of the parabola (A5) itself. The third piece is another tangent to parabola (A5) at a point ξ_1 such that $\beta \le \xi_1 \le \beta + \sqrt{4\alpha(1-f)}$. The fourth piece is the tangent of slope s_0 to the undriven parabola (A7). Note that η_0 is not smooth at ξ_0 (point of emergence of the water table) and ξ_e (the channel edge).

[42] It turns out that the diffusive term, though not present at zeroth order, acts to select a unique member from the one-parameter family of similarity solutions parameterized by ξ_1. The mechanism for the selection, verified by numerical methods, is unclear to us at this time. The selected similarity solution is one in which the third piece in equation (A8) (i.e., the tangent to the parabola (A5)) is missing; that is, ξ_1 assumes its upper limit $\xi_1 = \beta + \sqrt{4\alpha(1-f)}$. The slope of the sidewall of the channel in the undriven region is then simply

$$s_0 = \frac{1}{\sqrt{\alpha}}\left(1 + \sqrt{1-f}\right). \tag{A9}$$

The expressions for ξ_0 and ξ_e are simple as well,

$$\xi_0 = \beta + \sqrt{4\alpha(1-f)}, \quad \xi_e = \xi_0 + f/s_0 = \beta + \alpha s_0. \tag{A10}$$

Thus the asymptotic shape, illustrated in Figure 8, consists of a flat bottom, and curved parabolic flanks in the driven region followed by straight sidewalls of slope s_0.

[43] Besides selecting the unique self-similar shape, the diffusive term also acts to smooth slope discontinuities at ξ_0 and ξ_e. An exact expression for this smoothing can be obtained at the channel's edge ξ_e. In the vicinity of this point, the slope $s \equiv h_x$ is a hyperbolic tangent (verified by substitution),

$$s(x, t) = \frac{s_0}{2}\left(1 - \tanh\frac{s_0\alpha}{2}(x - vt)\right), \tag{A11}$$

moving with velocity (also given in equation (3))

$$v = \frac{a\xi_e}{\tau} = \delta + \lambda s_0, \tag{A12}$$

and smooth on a scale

$$R = \frac{2a}{s_0\alpha} = \frac{2\nu}{\sqrt{\lambda\mu}(1+\sqrt{1-f})}. \quad \text{(A13)}$$

Therefore, as we mentioned above, diffusion acts on a fixed scale R. The smoothing scale R also provides an independent way of estimating the diffusion constant ν from a static channel profile which is known to have resulted from evolution under steady driving conditions.

References

Baker, V. R., R. C. Kochel, J. E. Laity, and A. D. Howard (1990), Spring sapping and valley network development, in *Groundwater Geomorphology: The Role of Subsurface Water in Earth-Surface Processes and Landforms*, edited by C. G. Higgins and D. R. Coates, *Spec. Pap. Geol. Soc. Am.*, *252*, 235–265.

Boutreux, T., E. Raphael, and P. G. de Gennes (1998), Surface flows of granular materials: A modified picture for thick avalanches, *Phys Rev. E*, *58*(4), 4692–4700.

Culling, W. E. H. (1960), Analytic theory of erosion, *J. Geol.*, *68*, 336–344.

Dietrich, W. E., and T. Dunne (1993), The channel head, in *Channel Network Hydrology*, edited by K. Beven and M. J. Kirby, pp. 175–219, John Wiley, Hoboken, N. J.

Dietrich, W. E., D. G. Bellugi, L. S. Sklar, J. D. Stock, A. M. Heimsath, and J. J. Roering (2003), Geomorphic transport laws for predicting landscape form and dynamics, in *Prediction in Geomorphology*, *Geophys. Monogr. Ser.*, vol. 135, edited by P. R. Wilcock and R. M. Iverson, pp. 103–132, AGU, Washington, D. C.

Dunne, T. (1980), Formation and controls of channel networks, *Prog. Phys. Geogr.*, *4*, 211–239.

Dunne, T. (1990), Hydrology, mechanics, and geomorphic implications of erosion by subsurface flow, in *Groundwater Geomorphology: The Role of Subsurface Water in Earth-Surface Processes and Landforms*, edited by C. G. Higgins and D. R. Coates, *Spec. Pap. Geol. Soc. Am.*, *252*, 1–28.

Fleming, K., P. Johnston, D. Zwartz, Y. Yokoyama, K. Lambeck, and J. Chappell (1998), Refining the eustatic sea-level curve since the Last Glacial Maximum using far- and intermediate-field sites, *Earth Planet. Sci. Lett.*, *163*(1–4), 327–342.

Forterre, T., and O. Pouliquen (2003), Long-surface-wave instability in dense granular flows, *J. Fluid Mech.*, *486*, 21–50.

Horton, R. E. (1945), Erosional development of streams and their drainage basins: Hydrophysical approach to quatitative morphology, *Geol. Soc. Am. Bull.*, *56*, 275–370.

Howard, A. D. (1988), Groundwater sapping experiments and modelling, in *Sapping Features of the Colorado Plateau, a Comparative Planetary Geology Field Guide*, edited by A. D. Howard, R. C. Kochel, and H. E. Holt, pp. 71–83, Sci. and Tech. Inf. Div., NASA, Washington, D. C.

Howard, A. D. (1994), A detachment-limited model of drainage-basin evolution, *Water Resour. Res.*, *30*, 22,261–22,285.

Howard, A. (1995), Simulation modeling and statistical classification of escarpment planforms, *Geomorphology*, *12*, 187–214.

Howard, A. D., and C. F. McLane (1988), Erosion of cohesionless sediment by groundwater seepage, *Water Resour. Res.*, *24*, 1659–1674.

Jaggar, T. A. (1908), Experiments illustrating erosion and sedimentation, *Bull. Mus. Comp. Zool.*, *49*, 285–305.

Kochel, R. C., and J. F. Piper (1986), Morphology of large valleys on Hawaii: Evidence for groundwater sapping and comparisons with Martian valleys, *J. Geophys. Res.*, *91*(B13), E175–E192.

Kochel, R. C., A. D. Howard, and C. McLane (1985), Channel networks developed by groundwater sapping in fine-grained sediments: Analogs to some Martian valleys, in *Models in Geomorphology*, edited by M. J. Woldenberg, pp. 313–341, Allen and Unwin, Boston, Mass.

Kochel, R. C., D. W. Simmons, and J. F. Piper (1988), Groundwater sapping experiments in weakly consolidated layered sediments: A qualitative summary, in *Sapping Features of the Colorado Plateau, a Comparative Planetary Geology Field Guide*, edited by A. D. Howard, R. C. Kochel, and H. E. Holt, pp. 84–93, Sci. and Tech. Inf. Div., NASA, Washington, D. C.

Lobkovsky, A. E., W. Jensen, A. Kudrolli, and D. H. Rothman (2004), Threshold phenomena in erosion driven by subsurface flow, *J. Geophys. Res.*, *109*, F04010, doi:10.1029/2004JF000172.

McKean, J. A., W. E. Dietrich, R. C. Finkel, J. R. Southon, and M. W. Caffee (1993), Quantification of soil production and downslope creep rates from cosmogenic ^{10}Be accumulations on a hillsope profile, *Geology*, *21*, 343–346.

Montgomery, D. R., and W. E. Dietrich (1988), Where do channels begin?, *Nature*, *336*(6196), 232–234.

Montgomery, D. R., and W. E. Dietrich (1992), Channel initiation and the problem of landscape scale, *Science*, *255*(5046), 826–830.

Ni, W. J., and H. Capart (2006), Groundwater drainage and recharge by networks of irregular channels, *J. Geophys. Res.*, *111*, F02014, doi:10.1029/2005JF000410.

Overing, J. D., and F. C. Watts (1989), Soil survey of Walton county, technical report, Soil Conserv. Serv., U. S. Dep. of Agric., Washington, D. C.

Press, W. H., B. P. Flannery, S. A. Teukolsky, and W. T. Vettering (1986), *Combinatorial Minimization: Method of Simulated Annealing*, 1st ed., chap. 10.9, pp. 326–334, Cambridge Univ. Press, New York.

Reneau, S. L., W. E. Dietrich, M. Rubin, D. J. Donahue, and A. J. T. Jull (1989), Analysis of hillslope erosion rates using dated colluvial deposits, *J. Geol.*, *97*, 45–63.

Schörghofer, N., B. Jensen, A. Kudrolli, and D. H. Rothman (2004), Spontaneous channelization in permeable ground: Theory, experiment, and observation, *J. Fluid Mech.*, *503*, 357–374.

Schumm, S. A., M. D. Harvey, and C. C. Watson (1984), *Incised Channels: Morphology, Dynamics and Control*, Water Resour. Publ., Littleton, Colo.

Schumm, S. A., K. F. Boyd, C. G. Wolff, and W. J. Spitz (1995), A groundwater sapping landscape in the Florida panhandle, *Geomorphology*, *12*, 281.

Sellards, E. H., and H. Gunter (1918), Geology between the Apalachicola and Ocklocknee rivers, *10th Annual Rep.*, Fla. Geol. Surv., Tallahassee.

Willgoose, G., R. L. Bras, and I. Rodriguez-Iturbe 1991, A coupled channel network growth and hillslope evolution model: 1. Theory, *Water Resour. Res.*, *27*, 1671–1684.

Yalin, M. S. (1977), *Mechanics of Sediment Transport*, 2nd ed., Elsevier, New York.

Yoo, K., R. Amundson, A. M. Heimsath, and W. E. Dietrich (2005), Process-based model linking pocket gopher (*thomomys bottae*) activity to sediment transport and soil thickness, *Geology*, *33*(11), 917–920.

A. Kudrolli and B. E. Smith, Department of Physics, Clark University, Worcester, MA 01610, USA.

A. E. Lobkovsky, D. C. Mohrig, and D. H. Rothman, Department of Earth, Atmospheric and Planetary Sciences, Massachusetts Institute of Technology, Cambridge, MA 02139, USA. (leapfrog@mit.edu)